http://dx.doi.org/10.5012/bkcs.2011.32.9.3281

Characteristics of Ni/3d Series Transition Metal/γ-Al_2O_3 Catalysts and their Hydrogen Production Abilities from Butane Steam Reforming

Jun Su Lee, Byung-Hyun Choi,† Mi-Jung Ji,† and Misook Kang*

Department of Chemistry, College of Science, Yeungnam University, Gyeongsan, Gyeongbuk 712-749, Korea
**E-mail: mskang@ynu.ac.kr*
†Korean Institute of Ceramic Engineering & Technology (KICET), Geumcheon-gu, Seoul 153-801, Korea
Received May 19, 2011, Accepted July 20, 2011

The materials composed of the 3d series transition metals are introduced into the hydrocarbon steam-reforming reaction in order to enhance the H_2 production and abruptly depress the catalytic deactivation resulting from the strong sintering between the Ni component and the γ-Al_2O_3 support. The conventional impregnation method is used to synthesize the Ni/3d series metal/γ-Al_2O_3 materials through the sequentially loading Ni source and the 3d series metal (Ti, V, Cr, Mn, Fe, Co, Cu, and Zn) sources onto the γ-Al_2O_3 support. The Mn-loaded material exhibits a significantly higher reforming reactivity than the conventional Ni/γ-Al_2O_3 and the other Ni/3d series metal/γ-Al_2O_3 materials. Particularly the addition of Mn selectively improves the H_2 product selectivity by eliminating the formation of CH_4 and CO. The H_2 production is maximized at a value of 95% over Ni(0.3)/Mn(0.3)/γ-Al_2O_4(1.0) with a butane conversion of 100% above 750 °C for up to 55 h.

Key Words : Hydrogen production, Butane steam reforming reaction, Nickel/3d series metal/gamma-alumina, Manganese-loaded material

Introduction

The catalytic steam reforming of light hydrocarbons such as methane, methanol, ethanol, and dimethyl ether is of significant industrial importance for the production of hydrogen, and has attracted increasing interest in the context of the hydrogen economy. LPG, which is mainly composed of propane and butane gases, offers several advantages: it is easily handled and transported, and the existing infrastructure of the city gas is available for its use. Like propane, *n*-butane is a major constituent of LPG, and its conversion, in the presence of steam, affects the hydrogen yield according to the following equations[1-3]:

$$n\text{-}C_4H_{10} + 4H_2O = 4CO + 9H_2, \quad \Delta H^o\ 298 = 649.9\ \text{kJ/mol} \quad (1)$$

$$n\text{-}C_4H_{10} + 8H_2O = 4CO_2 + 13H_2, \Delta H^o\ 298 = 485.3\ \text{kJ/mol} \quad (2)$$

$$CO + H_2O = CO_2 + H_2, \quad \Delta H^o\ 298 = 41.2\ \text{kJ/mol} \quad (3)$$

Few studies have been carried out on the steam reforming of *n*-butane.[1-3] The commercial steam-reforming processes have used Ni-based catalysts because of their acceptably high activity and significantly lower cost in comparison to the alternative precious metal-based catalysts. However, these nickel-based catalysts are susceptible to deactivation through the deposition of carbon,[4-6] under the steam-reforming conditions, where the metal surfaces are covered with various CH_x intermediates. Without a fast steam gasification step to convert these intermediates to CO and H_2, these adsorbed CH_x species that are present on the Ni surface can undergo further dehydrogenation, polymerization, and rearrangement into highly stable carbon species that not only have a low reactivity toward the gasification reaction but can also dissolve into or encapsulate the Ni particles. In some cases, the dissolution of these carbon species leads to the growth of carbon whiskers, which eventually destroy the catalyst and plug the reactor. The abrupt catalytic deactivation that occurs at high temperatures above 650 °C is an especially serious problem for the $NiAlO_4$ catalysts because of the formation of the $NiAlO_3$ spinel structure that results from the strong sintering between Ni and Al. This deactivation caused the reactor to shutdown and the flow of the feed gases to reverse.[7,8]

To overcome these problems, some researchers have reported[9,10] that alkali (ex. MgO)- or noble metal (ex. Pt, Pd)-incorporated, Ni-based catalysts exhibited a stable activity for H_2 production, but some problems still exist in terms of the performance, lifetime, and cost of the catalyst. In our previous study,[11] Ag component was impregnated into Ni-$MgAl_2O_4$ in order to reduce the extent of the catalytic deactivation that was caused by the strong sintering between Ni and Al during the *n*-butane steam reforming. As a result, the H_2 production was maximized at 68% over Ni(9)/Ag(1)/$MgAl_2O_4$ at 700 °C for up to 53 h without any catalytic deactivation. However, the complexity in the manufacturing process of the catalyst and the differences in catalytic performance with respect to the loading order were still problems. Therefore, an excellent catalyst, which can be simply prepared and produces a high hydrogen gas yield, must be developed.

In this study, various Ni/3d series transition metal/γ-Al_2O_3 materials were examined in order to reduce the extent of the catalytic deactivation that was caused by the strong sintering between Ni and Al during the *n*-butane steam reforming. The effects of the 3d series transition metals on the catalytic

performance were considered, and the physicochemical properties of the materials were determined using XRD, H_2-TPR, and XPS analyses. The butane steam reforming reactions were conducted in the temperature range from 400-850 °C at intervals of 50 °C. The effects of the temperature, the steam/butane ratio, and the residence time on the activity and the selectivity of the catalyst were investigated, and the optimum conditions were discussed.

Experimental

Preparation of Ni/3d Series Transition Metal/γ-Al_2O_3 Materials. First, eight materials were prepared by loading the raw materials, including Ti, V, Cr, Mn, Fe, Co, Cu, and Zn, onto Al_2O_3 using the incipient wetness impregnation method, and these were compared to Ni/γ-Al_2O_3. In this synthesis process, 1.0 g of γ-Al_2O_3 (Sasol, 250-425 μm, 146 m^2/g) was impregnated with the 3d-metal nitrate ($M(NO_3)_2$ $6H_2O$, 30 wt % per γ-Al_2O_3 weight, Junsei Co., Japan) in 25 mL of isopropyl alcohol. The slurry was homogeneously stirred and evaporated below 70 °C for 30 min. The 3d-MAl_2O_4 materials were calcined at 500 °C for 1 h in air and impregnated with 30 wt % of nickel nitrate ($Ni(NO_3)_2 \cdot 6H_2O$, Junsei co. Japan) with respect to the 3d-MAl_2O_4 weight. The final samples were also evaporated at 70 °C for 30 min and dried in ambient air. These samples were heated in flowing air at a rate of 10 °C/min to 500 °C, and then isothermally held at 500 °C for at least 1 h. The various Ni/M/γ-Al_2O_3 materials were reduced with H_2 at 700 °C for 2 h and cooled to room temperature under argon gas before the butane-steam reforming reaction.

Characterizations of Ni/3d Series Transition Metal/ γ-Al_2O_3 Materials. The prepared Ni/3d-M/γ-Al_2O_3 materials were identified through powder X-ray diffraction analysis (XRD, model PW 1830 from Philips) with nickel-filtered Cu Kα radiation (40 kV, 100 mA) at 2-theta angles of 5-70°. The scan speed was 10°/min, and the time constant was 1 s. The Brunauer, Emmett and Teller (BET) surface area was measured using a Micrometrics ASAP 2000 instrument. All of the materials were degassed under vacuum at 120 °C for 1 h before the BET surface measurements. Then the samples were thermally treated at 300 °C for 30 min. The BET surface areas of the materials were measured through nitrogen gas adsorption using a continuous flow method with a mixture of nitrogen and helium as the carrier gas. The X-ray photon spectroscopy (XPS) measurements of Ni2p, 3d-M2p, and Al2p were recorded with an ESCA 2000 (VZ MicroTech, Oxford, UK) system that was equipped with a non-monochromatic AlKα (1486.6 eV) X-ray source. The powders were pelletized at 1.2×10^4 kPa for 1 min, and then the 1.0-mm pellets were stored overnight in a vacuum (1.0×10^{-7} Pa) in order to remove any water molecules from the surface prior to the measurements. The base pressure of the ESCA system was below 1×10^{-9} Pa. The experiments were conducted with a 200-W source power and an angular acceptance of ± 5°. The analyzer axis formed an angle of 90° with the specimen surface. The Shirley function was used to subtract the background in the XPS data analysis. The Ni2p, M3d, and Al2p XPS signals were fitted using the mixed Lorentzian-Gaussian curves. The H_2-TPR (temperature-programmed reduction) was conducted using the following method. About 0.3 g of the catalyst was pre-treated under a He flow (30 mL/min) at 700 °C for 2 h and then cooled to room temperature. The analysis was carried out at an H_2 (10 vol %)/N_2 flow rate of 30 mL/min while the temperature of the catalyst was raised from room temperature to 700 °C at a rate of 5 °C/min. The change in the hydrogen concentration was measured using a gas chromatograph (GC series 580, GOW-MAC) that was equipped with a TCD. The temperature-programmed oxidation (TPO) was performed using a Shimadzu DT-40 thermo-gravimeter in order to study the formation of the carbon on the material surface through the introduction of 5% oxygen in helium into the system after it was purged with helium. A 20 mg sample was placed in a sample pan and heated from 50 to 850 °C at a constant heating rate of 10 °C/min. High-purity air, composed of 21% oxygen and 79% nitrogen, was used as the O_2 gas source. The gas mixture was diluted to 5% in helium gas, and then the diluted gases flowed into the TPO system at a flow rate of 40 mL/min in order to combust the carbon that had accumulated on the catalyst after the reaction. The profiles were obtained in the same manner that was described for the TPO, and the coke content was calculated from the weight loss in the temperature range from 50 to 850 °C. α-Alumina (20 mg) was used as the reference. The amounts of CO and CO_2 were calibrated by injecting a known amount of the gases from a sample loop into an injection valve in the bypass line.

Apparatus for Butane Steam-reforming Reaction. The butane steam-reforming activity was measured over the nine materials, Ni/non, Ti, V, Cr, Mn, Fe, Co, Cu, and Zn/γ-Al_2O_3, in the temperature range of 400-850 °C for a the reaction time of 1 h at a steam-to-butane ratio of 1:4 with a GHSV (gas hourly space velocity) of 5500 h^{-1}. The butane gas was directly injected into the reactor, but the water was vaporized in a saturator at a temperature of above 100 °C before it was injected into the reactor. The resulting steam was injected into the catalytic reforming reactor using helium gas as the carrier gas. The *n*-C_4H_{10}:H_2O ratio of 1:4 corresponded to the flow rates of the butane gas and steam at values of 10 and 40 mL/min, respectively. The materials (0.5 g) were pelletized to 20-25 mesh, packed with a small amount of quartz wool in order to prevent it from moving in the 10-mm-diameter fixed-bed metal reactor, and vertically mounted inside the furnace**.** Before the testing, the catalysts were reduced in situ for 1 h at 700 °C with H_2 gas. Butane that was diluted with He was supplied from the cylinders, and the flow rate was adjusted using a flow meter before the gas was mixed in the mixing tank. The amount of water that was supplied for the vaporization was adjusted using a metering valve, and the water was introduced into the steam generator along with the mixture. This water was converted into vapor in the vapor generator and then sent to the thermal reactor in the mixed gaseous state. The inlet butane concent-

ration was held constant at 5 kPa (high purity C_4H_{10}), whereas the inlet steam concentration varied depending on the inlet H_2O/n-C_4H_{10} ratio requirements for each experiment (2.0, 4.0, and 8.0).

After the reactions, the exit gas mixture was transferred via the trace-heated lines to the analysis section, which consisted of a carbosphere column that was equipped with a Donam DS6200 (Donam company, Korea) GC and a mass spectrometer (MS). Gas chromatography was used to investigate the steady state condition experiments, whereas MS was used in the transient carbon formation experiments, where the exit gas was sampled using a quartz capillary and differential pumping. After the reaction, the catalysts were cooled to room temperature in argon gas and subjected to further characterization.

Results and Discussion

Characteristics of the Ni/3d Series Transition Metal/γ-Al_2O_3 Materials. The Ni/3d series transition metal/γ-Al_2O_3 materials that were both pre-treated and untreated with H_2 gas at 700 °C before the reaction were characterized using XRD in Figure 1. γ-Al_2O_3, which acted as the core metal in the materials, was observed as trace peaks at 2-theta angles of 47° and 68° in all of the samples,[12] but these peaks disappeared during the hydrogen reduction, except for the Ni/γ-Al_2O_3 material, possibly because the 3d series transition metals in the other materials completely covered γ-Al_2O_3, particularly due to the grain growth between the 3-d metals arising from the high temperature treatment. The diffraction lines of the 3d series transition metal oxide phases were observed in the XRD patterns of almost all of the materials, and particularly, the $NiMnO_x$ and $NiAlO_x$ composites that formed between Ni and the Mn or Al components were only observed in the Ni/Mn/γ-Al_2O_3 material. After the H_2 reduction, MO_x was partially reduced to the M^0 oxidation state in most of the materials, and the NiM alloy was also partially observed, particularly in Ni/Fe/γ-Al_2O_3. These results showed that the oxidation states of the main metal components existed between the oxidized and reduced forms.

Table 1 summarizes the physical properties of the nine Ni/3d-M/γ-Al_2O_3 materials. From the energy dispersive X-ray analysis, the loaded metals were different, with the Ni and 3-d metal surface atomic concentrations being relatively higher and lower, respectively. The atomic compositions of the exposed Ni were in the range of 20-59%, and the amount of inserted manganese element in Ni/Mn/γ-Al_2O_3 material was the smallest, indicating that Ni and Mn were sequentially covered on the alumina. Generally, the surface area exhibits a strong inverse relation to the particle size.

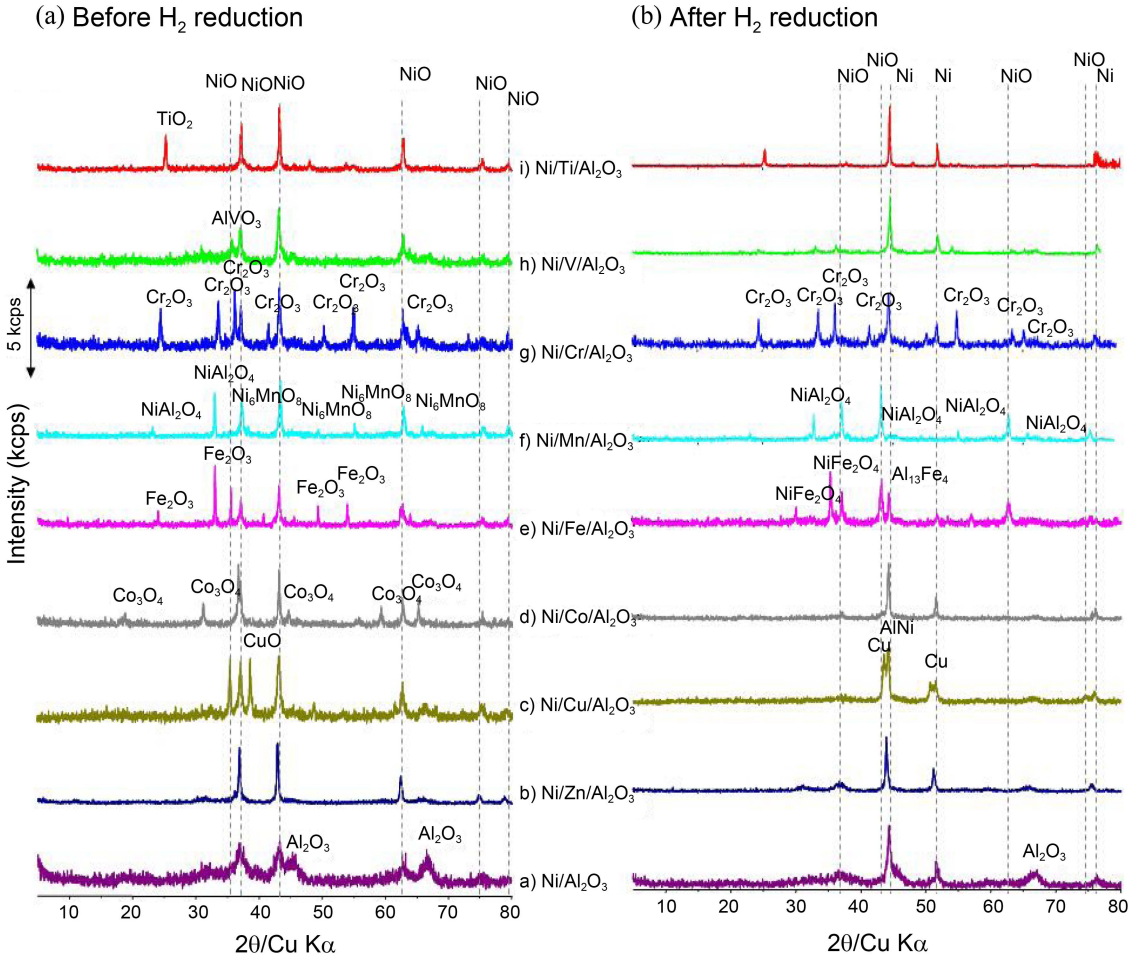

Figure 1. XRD patterns of the nine Ni/3d-M/γ-Al_2O_3 materials (a) before and (b) after the H_2 reduction.

Table 1. Physical properties, BET surface areas and atomic compositions for the nine Ni/3d-M/γ-Al_2O_3 materials

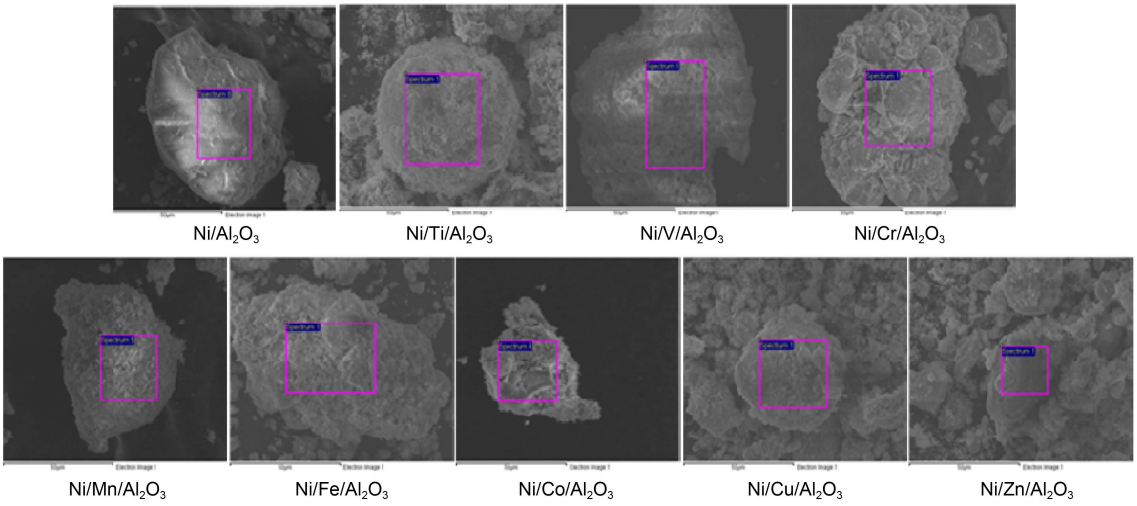

Catalysts	BET Surface area (m/g)	Atomic composition (mol %)			
		Al	Ni	M	O
Ni/Al_2O_3	108.4085	41.54	27.60	-	40.86
$Ni/Ti/Al_2O_3$	58.2504	6.11	59.80	9.97	24.11
$Ni/V/Al_2O_3$	59.8055	8.22	59.08	18.43	14.27
$Ni/Cr/Al_2O_3$	58.4997	11.99	25.41	29.70	32.90
$Ni/Mn/Al_2O_3$	50.4218	19.26	43.13	3.70	33.91
$Ni/Fe/Al_2O_3$	52.4967	15.73	37.95	20.37	25.96
$Ni/Co/Al_2O_3$	45.9168	16.76	27.66	26.59	28.99
$Ni/Cu/Al_2O_3$	51.0888	17.62	30.51	22.36	20.51
$Ni/Zn/Al_2O_3$	57.3261	26.17	20.61	21.11	32.12

However, this correlation was not observed in these results. The surface areas and the total pore volumes decreased to a greater extent in the bimetallic-loaded materials (45-59 m^2/g, Ni/3d metal/γ-Al_2O_3) than in the monometallic-loaded samples (108 m^2/g, Ni/γ-Al_2O_3). This decrease was strengthened by the impregnation of the 3d metals melted at high temperature and subsequently interfered with the Ni and Al particle spacing in the bulk material.

The H_2-TPR profiles of the nine Ni/3d-M/γ-Al_2O_3 materials are shown in Figure 2. The changes corresponding to the reduction of the 3d-metal oxides and the NiM alloy were observed in the H_2-TPR profiles. In general, the H_2-TPR results indicated that the peak area corresponded to the hydrogen uptake, and the peak at high temperatures corresponded to the reduction mechanism that was involved in the catalytic reaction. The reduction peak of NiO gradually shifted to lower temperatures with the additions of Mn, Co, V, Ti, and Zn, but was shifted to higher temperatures with the Fe and Cr additions. Additionally, the NiMn alloy reduction was observed at a low temperature of around 400 °C for Ni/Mn/γ-Al_2O_3. Generally, when the metal components were easily reduced during the hydrocarbon steam reforming reaction, the H_2-TPR curve of the metal component was observed at a lower temperature, which induced a higher hydrogen production.

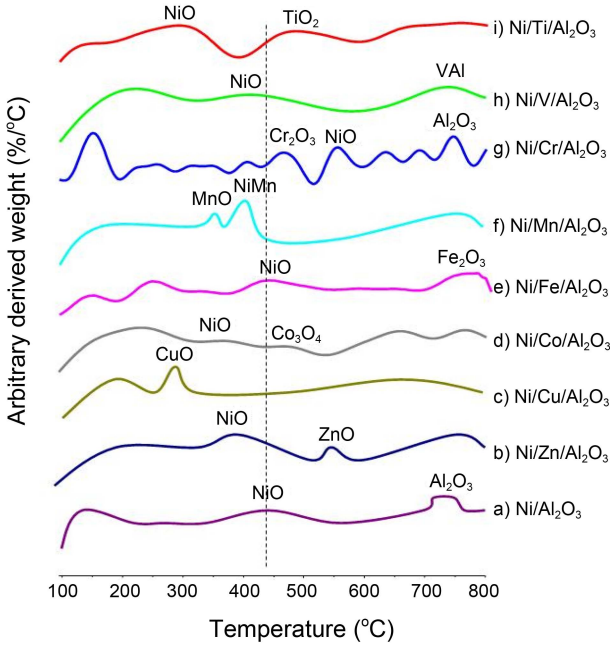

Figure 2. H_2-TPR curves of the nine Ni/3d-M/γ-Al_2O_3 materials.

Butane Steam Reforming Reaction over Ni/3d Series Transition Metal/γ-Al_2O_3 Materials. The butane steam reforming was carried out with 0.5 g of each of the nine materials, with various compositions of the Ni/3d-M/γ-Al_2O_3,

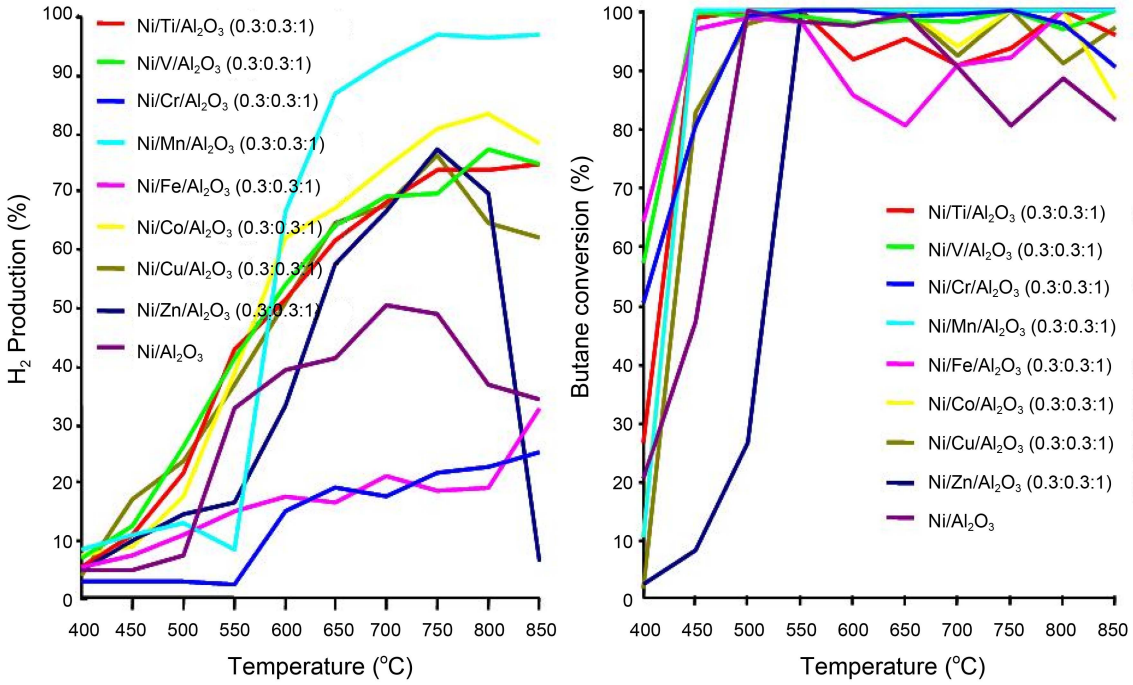

Figure 3. (a) H_2 production and (b) butane conversion over the nine Ni/3d-M/γ-Al_2O_3 materials with respect to the reaction temperature. Reaction conditions: 0.5 g sample, reaction temperature = 400-850 °C, GHSV = 5500 h^{-1}, and H_2O/*n*-C_4H_{10} = 4.0.

under the reaction conditions of a temperature of 400-850 °C, a GHSV of 5500/h, and a H_2O/*n*-C_4H_{10} ratio of 4.0. The *n*-C_4H_{10} conversion, H_2 production, and selectivity of CO and CO_2 were calculated using the following equations:

$$n\text{-}C_4H_{10}\ \text{conversion}\ (\%) = [C_{in}\ n\text{-}C_4H_{10} - C_{out}\ n\text{-}C_4H_{10}] / C_{in}\ n\text{-}C_4H_{10} \times 100$$

$$CO_2\ \text{selectivity}\ (\%) = C_{out}CO_2/[C_{out}\ CO_2 + C_{out}CO + C_{out}\ n\text{-}C_4H_{10} + C_{out}H_2] \times 100$$

$$n\text{-}CH_4\ \text{selectivity}\ (\%) = C_{out}\ n\text{-}C_4H_{10}/[C_{out}\ CO_2 + C_{out}CO + C_{out}\ n\text{-}C_4H_{10} + C_{out}H_2] \times 100$$

$$CO\ \text{selectivity}\ (\%) = C_{out}CO/[C_{out}\ CO_2 + C_{out}CO + C_{out}CH_4 + C_{out}H_2] \times 100$$

$$H_2\ \text{production}\ (\%) = \text{mol}\ H_2/[(\text{mol}\ n\text{-}C_4H_{10in} - \text{mol}\ n\text{-}C_4H_{10out}) - (\text{mol}\ H_2O_{in} - \text{mol}\ H_2O_{out})] \times 100\%$$

The reaction results below 400 °C were ignored because the butane conversion was less than 50%. Figure 3 compares the time-on-stream activity of the nine materials. In Figure 3(b), the butane conversions were above 90% at 500 °C for all of the materials, except Ni/Zn/γ-Al_2O_3 at 550 °C. On the other hand, the Ni/Mn/γ-Al_2O_3 material provided a significantly higher reforming reactivity than the other materials, with a conversion of 100% at 450 °C. The main products from the steam reforming over the Ni/3d-M/γ-Al_2O_3 materials were H_2, CO, CO_2, and CH_4, with trace amounts of other hydrocarbons. However, the addition of Mn decreased the carbon monoxide and selectively improved the H_2 production, because less methane and CO were emitted than the other materials. The proportion of methane emitted over Ni/Mn/γ-Al_2O_3 was less Ni/γ-Al_2O_3. The methanation of carbon dioxide and carbon monoxide on Ni materials has been observed in many studies.[13,14] The catalytic performances for the hydrogen production differed according to the added 3-d metals, and the selectivity decreased in the following order: Ni/Mn > Co > V > Ti > Zn > non-metal > Fe > Cr/γ-Al_2O_3 (Figure 3(a)). Although the H_2 production over Ni/γ-Al_2O_3 reached 48% at 700 °C, over Ni/Mn/γ-Al_2O_3 it was increased to 95% at 750 °C, which was quite remarkable compared to the other previously reported results. We also have previously reported [11] that the H_2 production and the butane conversion were 68% and 100%, respectively, over Ni(9)/Ag(1)/$MgAl_2O_4$ at the same conditions as in this study.

Figure 4 shows the product distributions obtained from the butane steam reforming over the Ni/γ-Al_2O_3 and Ni/Mn/γ-Al_2O_3 materials, which represented the highest catalytic performance in Figure 3. Unlike Figure 3, the H_2 selectivity (%) was calculated using $C_{out}H_2/[C_{out}CO_2 + C_{out}CO + C_{out}CH_4 + C_{out}H_2] \times 100\%$, and the product distributions were equivalent to a butane conversion of 100%. The reactions were conducted at C_4H_{10}:H_2O = 1:4, a reaction temperature of 750 °C, a reaction time of 1 h, and a GHSV of 5500 h^{-1}. Four species, H_2, CO, CO_2, and CH_4, were present in the product distribution. In this figure, the hydrogen selectivity was 42% for Ni/γ-Al_2O_3, but the highest hydrogen selectivity of more than 60% was obtained for Ni/Mn/γ-Al_2O_3, because of the decreased sintering between Ni and Al when Mn was incorporated into the middle of the catalyst, which enhanced the hydrogen selectivity during the butane conversion. Expectedly, the CO selectivity of the Ni/Mn/γ-Al_2O_3 slightly decreased to below 6%, whereas the CO_2 production increased to 8% compared to the non-3d metal catalyst. The

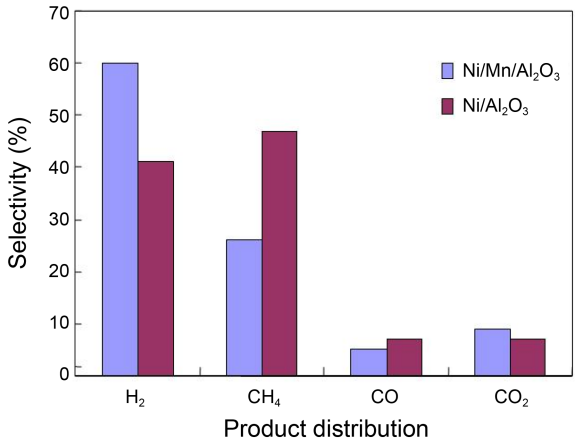

Figure 4. Production distribution during the butane steam reforming over Ni/γ-Al_2O_3 and Ni/Mn/γ-Al_2O_3. Reaction conditions: 0.5 g sample, reaction temperature = 750 °C, reaction time = 1 h, GHSV = 5500 h^{-1}, and H_2O/*n*-C_4H_{10} = 4.0.

presence of CO degraded the active catalyst due to catalytic poisoning.[15] Therefore, these results demonstrated that the introduction of the 3d transition metals between Ni and Al had a synergistic effect on the catalytic performance and decreased the sintering phenomenon, which caused the catalytic deactivation. A particularly strong influence was observed after the Mn addition.

Characteristics of Catalysts after Butane Reforming. Figure 5 compares the XRD patterns of the nine Ni/3d-M/γ-Al_2O_3 materials after a reaction time of 10 h at 700 °C. The main peak intensities after the reaction were weaker than the intensities before the reaction shown in Figure 1. The diffraction lines of the Ni^0 phase were observed at 2-theta angles of 43° and 52° in most of the materials, except for Ni/Zn/γ-Al_2O_3 and Ni/Cu/γ-Al_2O_3. Additionally, the NiAl alloys at 28° were not as pronounced in some materials

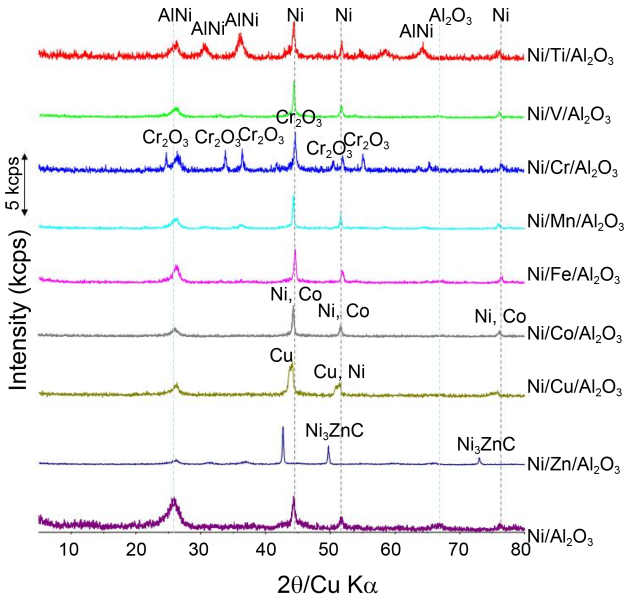

Figure 5. Comparison of the XRD patterns for the nine Ni/3d-M/γ-Al_2O_3 materials after the reaction.

compared to Ni/γ-Al_2O_3, indicating that the Ni components acted as active sites in the butane steam reforming reaction, as reported in many studies.[16,17] Additionally the peaks for the 3d metal phases were reduced in the oxidation state after the reaction in all of the materials, except for chromic oxide. Therefore, the 3d metal component also served as catalytic active sites similar to Ni, and additionally, the 3d metal components helped to retain the stability of the Ni crystallites and avoided their conglomeration in the butane steam reforming reaction. Thus, the Ni/3d-M/γ-Al_2O_3 materials exhibited a better stability than Ni/γ-Al_2O_3.

Figure 6 presents the typical survey and high-resolution spectra that were obtained from the quantitative XPS analysis of the Ni/γ-Al_2O_3 and Ni/Mn/γ-Al_2O_3 materials, which exhibited the highest catalytic performance in Figure 3. The survey spectra of the particles contained the Al2p, Ni2p, and Mn2p peaks in both before and after the butane steam reforming reactions. Additionally, the C1s peak, which corresponded to the carbon that accumulated over the surfaces of two catalysts, was observed after the butane steam reforming. The $Al2p_{3/2}$ spin-orbital photoelectron, which was assigned to the Al component in γ-Al_2O_3, was located at a binding energy of 74.4 eV for the two samples before the reaction. In general, larger binding energies and smaller peak widths indicate more oxidized states.[18] After the reaction, these peaks shifted to lower binding energies of 73.1 and 72.1 eV for Ni/γ-Al_2O_3 and Ni/Mn/γ-Al_2O_3, respectively, and the peaks broadened after the reaction. Generally, the $Ni2p_{3/2}$ and $Ni2p_{1/2}$ spectra in NiO are observed at 853.2 and 870.0 eV, respectively.[18] But the peak position can vary depending on the surrounding environment. The peaks were observed at 855.0 and 872.0 eV, respectively, after the reaction in this study. However, unfortunately, these peaks were not observed before the reaction for either catalyst because of noise in this study. Therefore, in this case, the changes of oxidation state of Ni before and after the reaction are difficult to determine.

Additionally, the same phenomenon occurred for Mn2p in Ni/Mn/γ-Al_2O_3. Generally, the $Mn2p_{3/2}$ spin-orbital, which was assigned to MnO, was located at a binding energy of 641.0 eV, and this peak shifted to 639 eV after the reaction, corresponding to the Mn^0 metal. These results indicated that the Al, Ni, and Mn ions were all reduced to lower oxidation states after the butane reforming, which confirmed the involvement of these ions in the oxidations of butane or other hydrocarbons, which occurred during the butane reforming reaction to produce CO_2. On the other hand, after the reaction the C1s region of the spectra were observed at 284.5 and 282.5 eV for carbon and carbide over Ni/γ-Al_2O_3 and Ni/Mn/γ-Al_2O_3, respectively. Thus, the carbon species that accumulated over the catalysts differed according to the metal components of the catalysts because of slight variations in the reaction mechanism.

The TPO measurements were carried out in order to determine the amount of carbon that was deposited on the nine Ni/3d-M/γ-Al_2O_3 materials, as shown in Figure 7. The deposited amount and species of carbons were closely

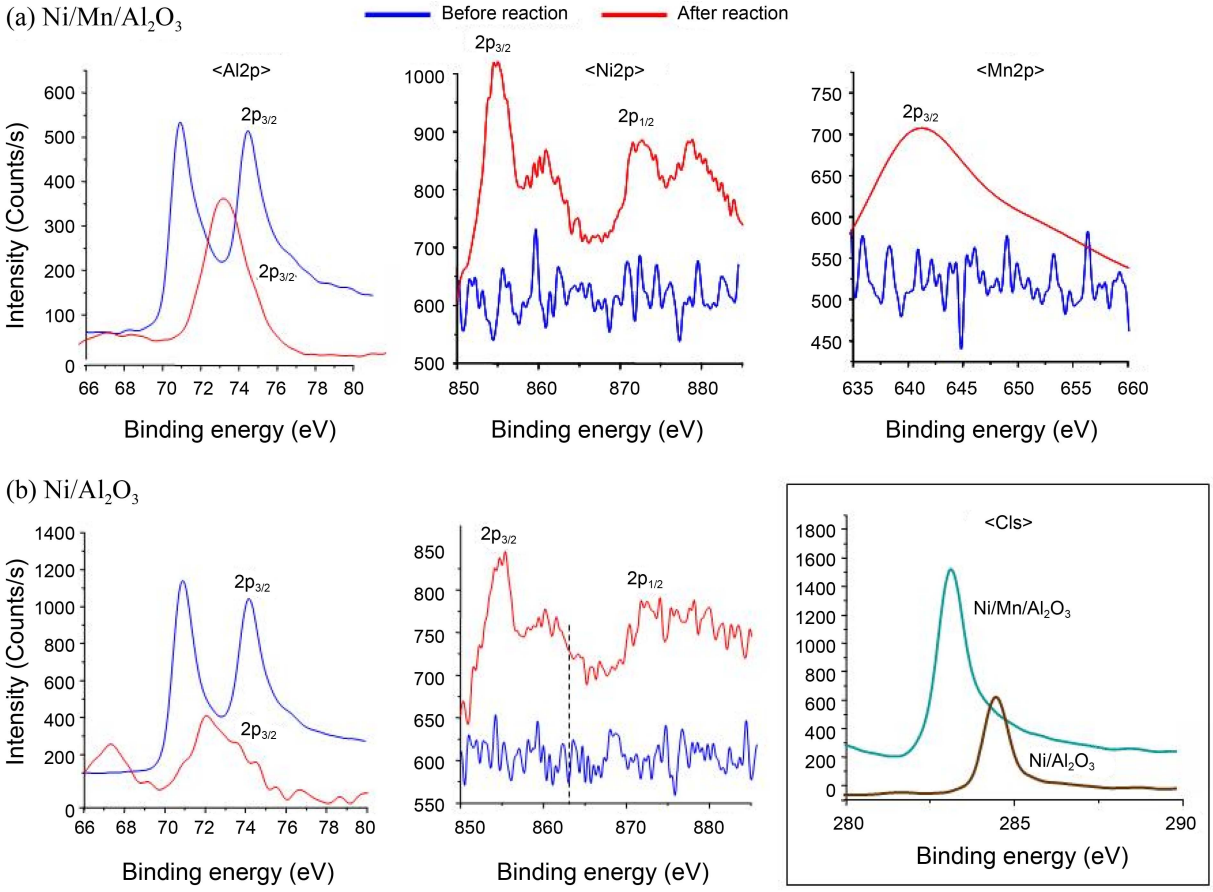

Figure 6. Comparison of the XPS curves for the Al2p, Mn2p, Ni2p, and C1s orbitals of the Ni/γ-Al_2O_3 and Ni/Mn/γ-Al_2O_3 materials before and after the reaction.

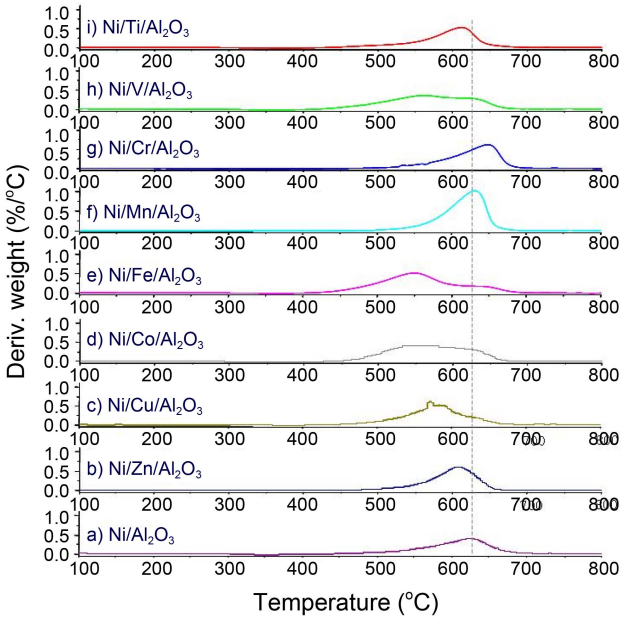

Figure 7. TPO profiles for the nine Ni/3d-M/γ-Al_2O_3 materials after the butane steam reforming.

related to the catalytic deactivation. Generally, the extent of the catalytic deactivation was reduced when smaller amounts of carbon were deposited. However, unfortunately, this behavior was not observed in this study. The deposited carbon amounts varied for the different 3d metal species, and the combustion temperatures for carbon were also different. The XPS results revealed that different types of carbon accumulated on the surface of the material. No decomposition of the deposited carbon was evident on the V, Fe, Co, and Cu-loaded materials at around 550-650 °C. With the addition of the Mn component to Ni/γ-Al_2O_3, the amount of deposited carbon slightly increased compared to Ni/γ-Al_2O_3, without changing the combustion temperature. This was probably because the butane steam reforming strongly and rapidly occurred evenly over the surfaces of all of the metals on the Ni/Mn/γ-Al_2O_4 samples.

Optimum Conditions for Butane Reforming. Figure 8 shows the catalytic performances for the butane reforming reaction over the Ni/Mn/γ-Al_2O_3 materials with various Ni:Mn ratios of 0.1:0.3, 0.3:0.1, and 0.3:0.3 at a GHSV = 5500 h^{-1} and a *n*-C_4H_{10}:H_2O mole ratio = 1:4. Both the butane conversion and the H_2 yield improved in almost all of the Mn-loaded samples compared to the catalyst without the Mn component because of the synergistic effect. When the Ni loading was larger than amount of Mn, the reaction occurred at a higher temperature and the H_2 production was minimized. Particularly, the butane conversion was about 100% at 450 °C for the catalyst with the atomic ratio of

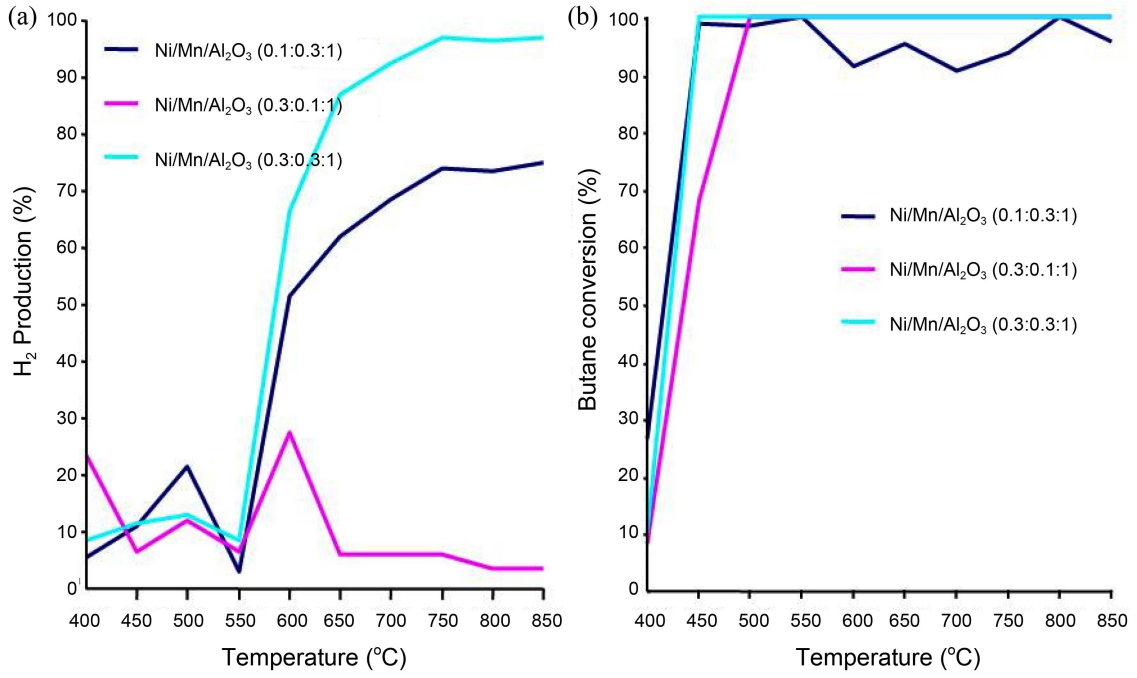

Figure 8. Butane conversion and H_2 production over Ni/Mn/γ-Al_2O_3 according to the molar ratio of Ni/Mn: (a) H_2 production and (b) butane conversion.

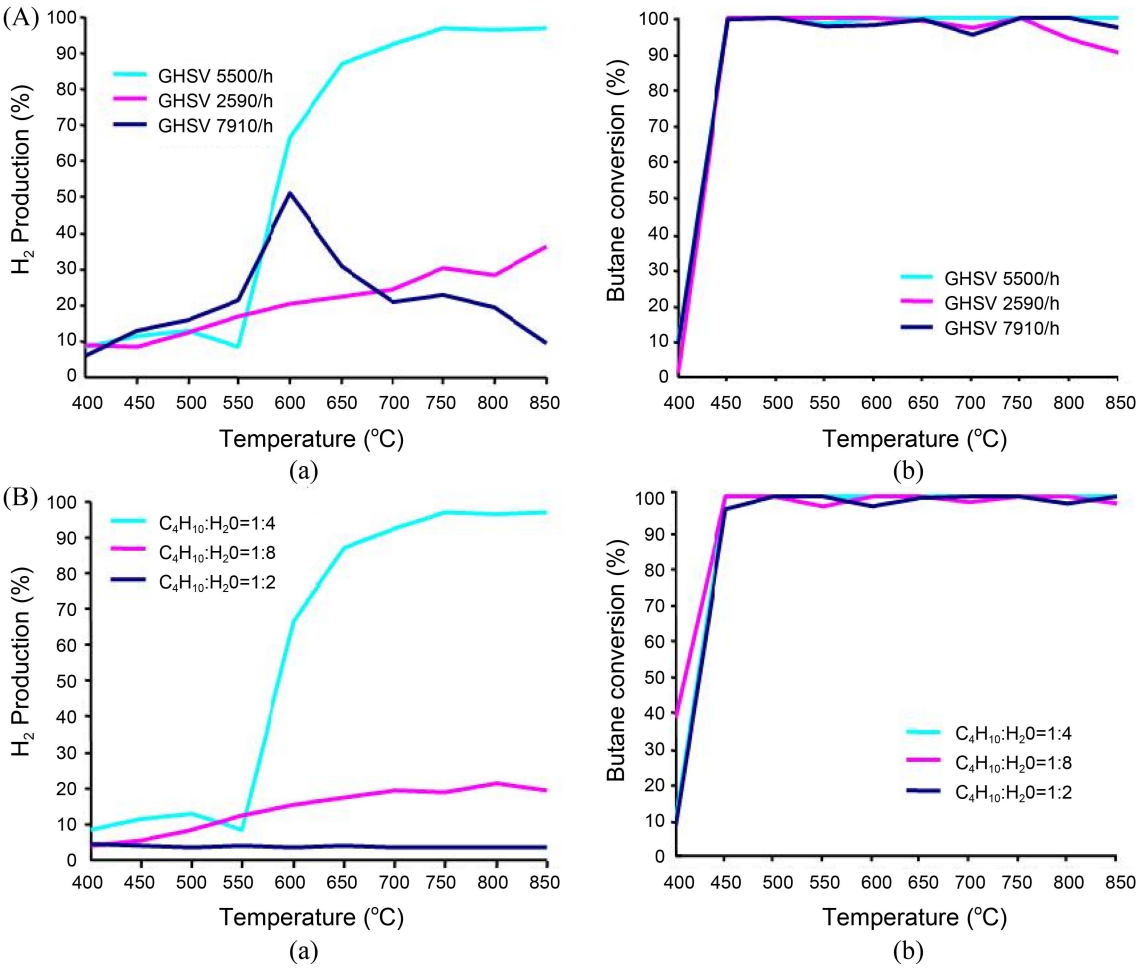

Figure 9. (a) H_2 production and (b) butane conversion over Ni/Mn/Al_2O_3 with respect to (A) the GHSV and (B) the molar ratio of C_4H_{10}/H_2.

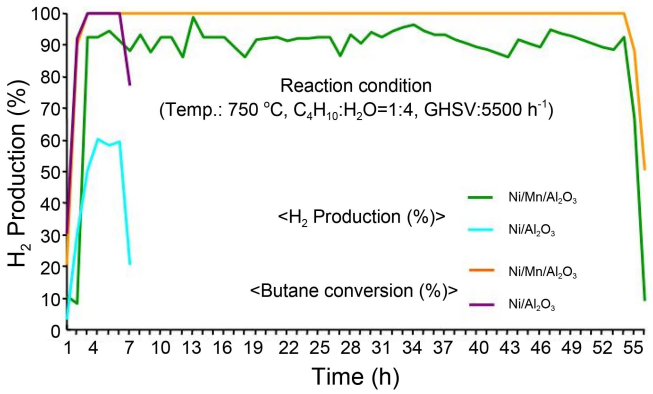

Figure 10. Catalytic deactivation tests over Ni/γ-Al_2O_3 and Ni/Mn/γ-Al_2O_3. Reaction conditions: 0.5 g sample, reaction temperature = 750 °C, GHSV = 5500 h^{-1}, and H_2O/*n*-C_4H_{10} = 4.0.

Ni:Mn = 0.3:0.3, and the butane was selectively converted to hydrogen with a high yield of 95% from 750 to 850 °C. Otherwise, the catalytic performance was rather poor when too much Mn was added. The best performance was observed for the Ni(0.3)/Mn(0.3)/γ-Al_2O_3(1.0) catalyst.

Figure 9 A and B show the catalytic performances for the butane steam reforming reaction over Ni(0.3)/Mn(0.3)/γ-Al_2O_3(1.0) with respect to changes in the GHSV and the butane(*n*-C_4H_{10})/steam(H_2O) ratio, respectively. Figure A shows that the H_2 production significantly improved at a reaction temperature 550 °C to 95% at 750 °C with a butane conversion of 100% at a GHSV of 5500 h^{-1}. However, the catalytic performance decreased at lower or higher GHSVs. The optimum condition was *n*-C_4H_{10}:H_2O=1:4 and 95% of the hydrogen was emitted at 750 °C with a butane conversion of 100%, as shown in Figure B. However, the hydrogen production decreased above this ratio. Therefore, the optimal reaction conditions for the production of H_2 over the Ni(0.3)/Mn(0.3)/γ-Al_2O_3(1.0) catalyst were GHSV=5500 h^{-1}, *n*-C_4H_{10}:H_2O mole ratio = 1:4, and reaction temperature=750 °C according to the active response.

Finally, the catalytic deactivation was tested for the Ni/γ-Al_2O_3 and Ni/Mn/γ-Al_2O_3 catalysts, and the results are shown in Figure 10. The difference in the H_2 production between these two catalysts was 0.3% depending on the presence or absence of Mn. The catalytic lifetime was greatly improved in Ni/Mn/γ-Al_2O_3 compared to the material without Mn. The catalytic deactivation remarkably progressed after only 7 h over Ni/γ-Al_2O_3, and both the H_2 production and the butane reforming rapidly decreased. The rapid deactivation over Ni/γ-Al_2O_3 indicated that the initial catalyst deactivation resulted from a combination of the steam-induced nickel sintering and the carbon deposition. However, the apparent deactivation rate was far lower for the Mn-promoted catalyst, and its higher butane conversion of 100% and H_2 yield of 85-98% continued for up to 55 h. Thus, the improved stability that was achieved with the Ni/Mn sample at the slower deactivation rate could not unequivocally be attributed to the carbon formation.

Conclusion

In this present work, the 3d transition metals were added between Ni and Al in an attempt to decrease the catalytic deactivation that was induced by the strong sintering between Ni and Al during butane steam reforming, while simultaneously improving the catalytic activity. The study results confirmed that the catalytic performances differed with respect to the 3d metal species. Particularly, the addition of the Mn component maybe helped to retain the stability of the Ni-Al crystallites and prevent their conglomeration during the butane steam reforming. The catalytic performance decreased in the following order: Ni/Mn > Co > V > Ti > Zn > non-metal > Fe > Cr/γ-Al_2O_3. The H_2 production and butane conversion reached 95% and 100%, respectively, over Ni(0.3)/Mn(0.3)/γ-Al_2O_3(1.0) for up to 55 h without any catalytic deactivation. The optimal operation conditions were identified as a reaction temperature of 750 °C, a gas hourly space velocity (GHSV) of 5500 h^{-1}, and a feed ratio of n-C_4H_{10}:H_2O of 1:4.

Acknowledgments. This work was supported by the New & Renewable Energy of the Korea Institute of Energy Technology Evaluation and Planning (KETEP) grant funded by the Korea government Ministry of Knowledge Economy (No. 2010T100100622).

References

1. Avcl, A. K.; Önsan, Z. I.; Trimm, D. L. *Appl. Catal. A* **2001**, *216*, 243.
2. Avcl, A. K.; Trimm, D. L.; Aksoylu, A. E.; Önsan, Z. I. *Appl. Catal. A* **2004**, *258*, 235.
3. Chin, Y. H.; King, D. L.; Roh, H. S.; Wang, Y.; Heald, S. M. *J. Catal.* **2006**, *244*, 153.
4. Xu, J.; Chen, L.; Tana, K. F.; Borgna, A.; Saeys, M. *J. Catal.* **2009**, 261, 158.
5. Kroll, V. C. H.; Swaan, H. M.; Mirodatos, C. *J. Catal.* **1996**, *161*, 409.
6. Rostrup-Nielsen, J. R.; Anderson, J. R.; Boudart, M. *Catalytic Steam Reforming, Catalysis Science and Technology*; Springer-Verlag: Berlin, 1984, Vol. 5, chap. 1.
7. Swaan, H. M.; Kroll, V. C. H.; Martin, G. A.; Mirodatos, C. *Catal. Today* **1994**, *21*, 571.
8. Wei, J.; Iglesia, E. *J. Catal.* **2004**, *224*, 370.
9. Gökaliler, F.; Göçmen, B. A.; Aksoylu, A. E. *Int. J. Hydrogen Energy* **2008**, *33*, 4358.
10. Sato, K.; Nagaoka, K.; Nishiguchim, H.; Takita, Y. *Int. J. Hydrogen Energy* **2009**, *34*, 333.
11. Jeong, H.; Kang, M. *Appl. Catal. B* **2010**, *95*, 446.
12. Nie, X.; Meletis, E. I.; Jiang, J. C.; Leyland, A.; Yerokhin, A. L.; Matthews, A. *Surf. Coat. Tech.* **2002**, *149*, 245.
13. Hirano, H.; Tanaka, K. I. *J. Catal.* **1992**, *133*, 461.
14. Du, G.; Lim, S.; Yang, Y.; Wang, C.; Pfefferle, L.; Haller, G. L. *J. Catal.* **2007**, *249*, 370.
15. Ma, L.; Trimm, D. L.; Jiang, C. *Appl. Catal. A* **1996**, *138*, 275.
16. Sago, F.; Fukuda, S.; Sato, K.; Nagaoka, K.; Nishiguchi, H.; Takita, Y. *Int. J. Hydrogen Energy* **2009**, *34*, 8046.
17. Seo, J. G.; Youn, M. H.; Song, I. K. *Int. J. Hydrogen Energy* **2009**, *34*, 1809.
18. Mazzieri, V.; Coloma-Pascual, F.; Arcoya, A.; L'Argentière, P. C.; Fígoli, N. S. *Appl. Surf. Sci.* **2003**, *210*, 222.